Volume 19, No 2 | International Journal of Radiation Research, April 2021

A new algorithm for dose calculation in heterogeneous lung phantoms under condition of small field size

P. Yang[1], Z. Chen[1], Q. Lei[2], C. Yin[1], S. Zhang[1], Z. Wu[1], C. Gou[1]*

[1]*Sichuan University, Chengdu, Sichuan, China*
[2]*Nuclear Power Institute of China, Chengdu, Sichuan, China*

► ***Original article***

Corresponding authors:
Dr. Chengjun Gou,
E-mail:
GOUCJSCU720@scu.edu.cn

Revised: April 2020
Accepted: May 2020

Int. J. Radiat. Res., April 2021; 19(2): 259-267

DOI: 10.29252/ijrr.19.2.259

ABSTRACT

Background*:** Current dose algorithms, such as the collapsed cone convolution algorithm and anisotropic analytical algorithm, are widely used in commercial treatment planning systems. Nevertheless, it is difficult to calculate the dose distribution of heterogeneities for small fields by using these algorithms, because of the electronic disequilibrium. However, contemporary treatment uses small beamlets more and more frequently, such as stereotactic body radiation therapy and intensity-modulated radiation therapy. In this study, a new inhomogeneity method in lung medium for small fields was presented. ***Materials and Methods: Inhomogeneous lung phantoms for different small fields were established, and different locations and thicknesses of lung media in inhomogeneous phantoms were also considered. The Monte Carlo code EGSnrc was used to calculate the density factor and the percentage depth-dose (PDD) distribution of lung phantoms. The PDDs were also calculated with the new algorithm, and then differences in the PDDs were determined. ***Results:*** The comparison shows that there is a good agreement between the new algorithm and the Monte Carlo code in different energy. The discrepancies of the three field sizes were less than 3%. With an increase in field size, the discrepancies were less than 1%. Even with changes in the location and thickness of the lung media in inhomogeneous phantoms, the discrepancies were always less than 1%. ***Conclusion:*** The comparative results revealed the effectiveness of the new algorithm in calculating depth-dose distribution, under different conditions, and that it can meet the requirements for calculating percentage depth dose distribution.

Keywords: *Dose algorithm, small fields, inhomogeneous lung phantom, Monte Carlo simulation, percentage dose depth distribution.*

INTRODUCTION

Nowadays, with the rapid development of radiotherapy techniques (RTs), small treatment fields are used more frequently, such as in stereotactic radiotherapy (SRT) [1] and intensity-modulated radiation therapy (IMRT) [2]. These radiotherapy techniques can use small fields to reduce the irradiation dose to healthy tissue to a much lower dose than occurs in conventional conformal therapy.

Nevertheless, with the decrease in the irradiation field size, measurements become difficult, and in some situations impossible, due to the size of the detector. Because of different densities in the human body, radiation transport will produce varying dose distributions [3]. Moreover, with the decrease in the field size, electronic equilibrium may not be established [4, 5].

A dose calculation algorithm should be accurate within 3%. Many studies which evaluate the accuracy of various algorithms present in commercial treatment planning

[Downloaded from mail.ijrr.com on 2026-11-12]

[DOI: 10.52547/ijrr.19.2.3]

systems (TPSs) have calculated dose distribution in heterogeneous phantoms [6-11]. In 2006, Knöös *et al.* [6] suggested classification types "a" and "b". In 2017, Fogliata *et al.* [7], suggested adding a type "c". The type "a" algorithm, such as the equivalent pathlength algorithm (EPL), the Batho algorithm and all pencil beam (PB) convolution algorithms, do not consider electron transport. They deal with inhomogeneities using a correction evaluated on the one-dimensional path length along the fan lines. Using the Batho algorithm, du Plessis *et al.* [8] showed absorbed dose deviations of 10–20% in lung tissue of varying density for a 2×2 cm^2 field. With the PB algorithm, the deviations can also be up to 5% for 4MV beams, increasing with energy. For type "b" algorithms, such as the anisotropic analytical algorithm (AAA), the collapsed cone convolution (CCC) and the multigrid superposition (MGS), electron transport is considered. As a result, they can reduce the absorbed dose deviation compared to the type "a" class. However, with a decrease in field size, the effect of electronic disequilibrium is more important. For example, if the field size is above 3×3 cm^2 and lateral electronic equilibrium is achieved, the CCC algorithm is quite accurate. The maximum dose deviation is 5%, and the average dose deviation is less than 3% [9, 10]. On the other hand, if the field size is less than 3×3 cm^2, the CCC algorithm is not accurate and within the lung tissue is overestimated, so the differences are more obvious with increasing energy. The type "c" class, such as the Acuros,[11] Linear Boltzmann Transport Equation LBTE solver and Monte Carlo (MC) algorithms, can accurately explain the physics generating the dose absorption process and have a great degree of agreement with the measurement. Researchers always use the MC code to evaluate dose algorithms or calculate the convolution kernel [12].

In this research, a new algorithm for calculating the percentage depth dose distribution of inhomogeneous lung phantoms for small irradiation fields is presented. This algorithm can calculate the dose distribution of heterogeneous lung phantoms for different small fields, it is suitable for different energy and its accuracy does not vary with the thickness or location of lung tissues in the phantom. Moreover, the procedure simplifies the complexity of the calculation by using the depth-dose distribution of homogeneous water phantom.

MATERIALS AND METHODS

Dose calculation principle

When incident photons with an energy of E_0 are perpendicular to the surface of a homogeneous phantom, the transport equation of the photons in the homogeneous phantom is defined as eq. (1) [13]:

$$\mu\frac{\partial\Phi}{\partial Z} = -\sum(E)\Phi(Z,\mu,E) + \int_{4\pi} d\vec{\Omega}' \int_{E}^{E_0} dE'\,\Phi(Z,\mu',E')\,K\left(E',E;\vec{\Omega}\cdot\vec{\Omega'}\right) + \delta(Z)\delta(E-E_0)\delta(1-\mu)/2\pi \quad (1)$$

$\Phi(Z,\mu,E)$ is the fluence distribution of the photons, $\Phi(Z,\mu,E)dsdEd\Omega$ represents the number of photons at depth Z with energy between E and $E + dE$, and directions between Ω and $\Omega + d\Omega$ passing through a small area $d\vec{s}$ perpendicular to Ω direction, μ denotes the cosine of the direction of incident photons and the direction of rays perpendicular to the medium surface and $K(E',E;\ \Omega\cdot\Omega')\ dE'\ d\Omega'$ represents the transition probability of a photon passing through a medium with a unit mass thickness. $\sum$€ is the linear attenuation coefficient of photons with energy of E:

$$\sum(E) = \frac{N_A}{A}\cdot\sigma_{tot}\cdot\rho \quad (2)$$

N_A is the Avogadro constant, A is the atomic weight of this medium and σ_{tot} represents the total cross-section [14].

Eq. (1) can be solved with the characteristic line method [13] the solution to eq. (2) is defined as eq. (3):

$$\Phi(Z, E)=\Phi(0)e^{-\sum(E)\cdot Z} \quad (3)$$

[Downloaded from mail.ijrr.com on 2026-11-12]

[DOI: 10.52547/ijrr.19.2.3]

Φ(Z, E) represents the photon fluence at depth *Z*, and Φ_0€ represents the incident photon fluence. The secondary electrons produced by primary photons are defined as eq. (4):

$$S(Z,E) = \Phi(Z,E)dS \cdot \frac{N_A}{A}\rho \cdot dZ \cdot \sigma_{tot} \quad (4)$$

These electrons will keep transporting in the medium, and some of the electrons will interact with the nucleus or electrons of the medium and deposit energy. The formula of dose deposition is defined as eq. (5):

$$D_1 = \frac{S(Z,E)\cdot L(E)dZ}{\Delta m} = \frac{\Phi(Z,E)dS\cdot\frac{N_A}{A}\rho\cdot dZ\cdot\sigma_{tot}\cdot L(E)dZ}{\rho dV} = \Phi(Z,E)\frac{N_A}{A}\sigma_{tot}\cdot L(E)dZ \quad (5)$$

L(E) represents the restricted stopping power of electrons with energy *E*, which means the energy absorbed by the matter and the energy generated by the ionization and excitation of charged particles when they travel per unit distance.

The secondary electrons with low energy will deposit all the energy at the point of interaction. This part of the energy deposition is noted as D_1. Combining with eq. (5), D_1 can be simplified as:

$$D_1^{lung}(Z,E) = \Phi(Zeff,E)_{water}\left(\frac{N_A}{A}\cdot\sigma_{tot}\right)_{lung}\cdot L(E)_{water}\frac{L(E)_{lung}}{L(E)_{water}}dZ \quad (6)$$

Where $Zeff = \frac{\sum(E)_{lung}}{\sum(E)_{water}}\cdot Z$ in eq. (6).

On the other hand, if the electrons have higher energy, only part of their energy will deposit at the point of interaction, and another part will deposit at a deeper place. This part of the dose deposition can be expressed as D_2, and the dose deposition at distance *Z* can be divided into two parts:

$$D(Z,E)=D_1+D_2. \quad (7)$$

Thus, the dose distribution at depth of Z can be calculated by eq. (6) and eq. (7):

$$D_{lung}(Z,E) = D_1^{water}(Z_{eff},E)\cdot\frac{L(E)_{lung}}{L(E)_{water}} + D_2^{lung}(Z,E)$$
$$= D^{water}(Z_{eff},E)\cdot\frac{L(E)_{lung}}{L(E)_{water}} - D_2^{water}(Z_{eff},E)\cdot\frac{L(E)_{lung}}{L(E)_{water}} + D_2^{lung}(Z,E) \quad (8)$$

D_{water} (Z_{eff},E) means the dose distribution in a water phantom. $D_2^{water}(Z_{eff},E)\cdot\frac{L(E)_{lung}}{L(E)_{water}}$ And $D_2{}^{lung}$ (Z,E) mean the primary and secondary electrons from the front point in water and lung and the electronic disequilibrium. Therefore, we consider this part to be a function of D_1, and the relative coefficient is called the density factor.

$$D_{lung}(Z,E) = D_{water}(Z_{eff},E)\cdot\frac{L(E)_{lung}}{L(E)_{water}} + C\cdot\frac{L(E)_{lung}}{L(E)_{water}}\cdot D_{water}(Z_{eff},E) = D_{water}(Z_{eff},E)\cdot(1+C)\cdot\frac{L(E)_{lung}}{L(E)_{water}}. \quad (9)$$

C is considered the density factor in eq. (9).

Density factor

The density factor can be accepted by experimental measurement and Monte Carlo simulation; in this section, all the density factors are calculated using MC code.

Homogeneous water phantoms and homogeneous lung phantoms were modelled. The size of the phantom was 40×40×40 cm^3, and the scoring voxel was 0.25×0.25×0.25 cm^3. The lung densities were 0.1g/cm^3 and 0.5g/cm^3. When the lung density was 1g/cm3, the dose distributions were considered to be the same as those of water. The field sizes were 0.25×0.25 cm^2, 1×1 cm^2 and 3×3 cm^2. The energy of incident photons were set to 2 MeV and 6MV. The density factors were obtained using eq. (9) and considered to be the reference values.

When calculating the depth-dose distribution of heterogeneous lung phantoms, first, the density factors under different fields were obtained using Lagrange interpolation. Then, the Lagrange interpolation was used again to calculate the density factor at the corresponding density. Finally, the depth-dose distribution was calculated using eq. (9).

Monte Carlo simulations

Monte Carlo simulations were performed

[Downloaded from mail.ijrr.com on 2026-11-12]

[DOI: 10.52547/ijrr.19.2.3]

using the (DOSXYZnrc) user code of EGSnrc from the NRCC group in Ottawa, Canada [15, 16]. The energy of incident photons was set to 2 MeV and 6 MV. The 6 MV photon beams were produced by medical linear accelerators and its spectra was from Mohan *et al.* [17] the global cut-off photon energy was 0.01 MeV, and the cut -off energy for electrons was 0.521 MeV. Histories were set to 10^9.

To measure the accuracy of the algorithm, several heterogeneous lung phantoms were developed. The size of the phantoms was 40×40×40 cm^3, and the scoring voxel was 0.25×0.25×0.25 cm^3. Figure 1 shows the front view of the different phantoms. In figure 1a, the lung density is 0.26g/cm^3. The field sizes are 0.25×0.25 cm^2, 1×1cm^2 and 2×2 cm^2. The composition of the phantom from top to bottom is water (15cm), lung (10cm), and water (15cm). In figure 1(b-e), the lung density is 0.26 g/cm^3 and the field size is 0.25×0.25cm^2. In figure 1b, the composition of the phantom from top to bottom is water (5cm), lung (10cm), and water (25cm). In figure 1c, the composition of the phantom from top to bottom is water (25cm), lung (10cm), and water (5cm). In figure 1d, the composition of the phantom from top to bottom is water (15cm), lung (5cm), and water (20cm). In figure 1e, the composition of the phantom from top to bottom is water (15cm), lung (15cm), and water (10cm).

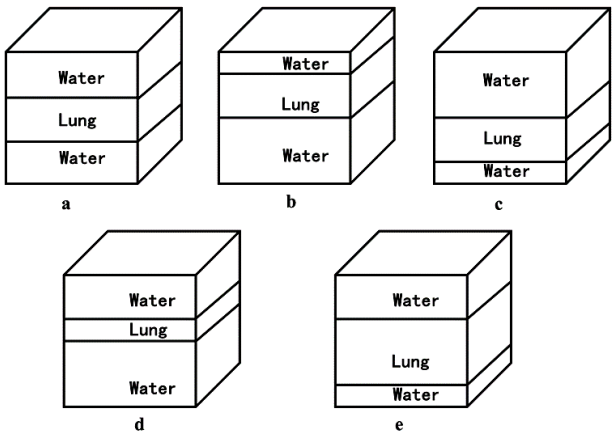


Figure 1. Different types of heterogeneous phantoms. **(a)** water (15cm), lung (10cm), water (15cm). **(b)** water (15cm), lung (10cm), water (15cm). **(c)** water (15cm), lung (10cm), water (15cm). **(d)** water (15cm), lung (10cm), water (15cm). **(e)** water (15cm), lung (10cm), water (15cm). The lung density in each phantom is 0.26g/cm^3.

The percentage depth-dose distributions (PDDs) of these heterogeneous lung phantoms calculated using DOSXYZnrc code are considered to be the reference values. The PDDs also calculated using the new algorithm. The new algorithm is performed by the C programming language. All programs are implemented on the Windows operating system. The dose deviation (DD) is defined as eq. (10) [18]:

$$DD = \frac{D_{Z,MC} - D_{Z,New\ Algorithm}}{D_{max,MC}} \quad (10)$$

D_z, represents the absolute dose at the depth of Z, D_{max} represents the max absolute dose in the phantom.

RESULTS

Figure 2 shows that the value of density factor varies with depth. This graph can be divided into two parts. The descent region represents the build-up of electrons; in this region, the value decreases until the peak dose point is come out. The flat region represents the charged particles' equilibrium and the value trends of slow and uniform decline; this part does not change significantly, so taking the average of these values as the density factor.

Figure 3 shows that the percentage depth-dose curves for the heterogeneous lung phantom calculated by MC simulations using DOSxyznrc code in comparison with those obtained with the new algorithm. The discrepancy of percentage depth-dose within the water-lung interface is described in table 1. There is a dose drop at the interface of the anterior portion of the lung with the water. During this build-down region, the values obtained by the new algorithm are all lower than those obtained by MC, as shown in figure 3 and table 1. These data have a large gradient descent, and the largest discrepancy is 17% in figure 3A. Subsequently, the dose decreases slowly during the region of lung tissue. This is the main region with which we are concerned, called the valley region [9]. In this valley region, there is great agreement between MC code and the new algorithm. The discrepancies in this region are

[Downloaded from mail.ijrr.com on 2026-11-12]

[DOI: 10.52547/ijrr.19.2.3]

all less than 3% in table 1. Moreover, with the increase in field size, the results can be more accurate. All dose deviations are basically less than 1%, the largest deviation is 1.37% and the minimum deviation is 0.1% for 2×2 cm² filed. Then there is subsequent dose build-up immediately distal to the lung tissue, and a dose enhancement on the distal side of the lung tissue. The values obtained by the new algorithm are all higher than those obtained by MC. The largest discrepancy is 12% in figure 3C. After that, the PDD obtained by the two methods is almost the same, until the distal to the phantom.

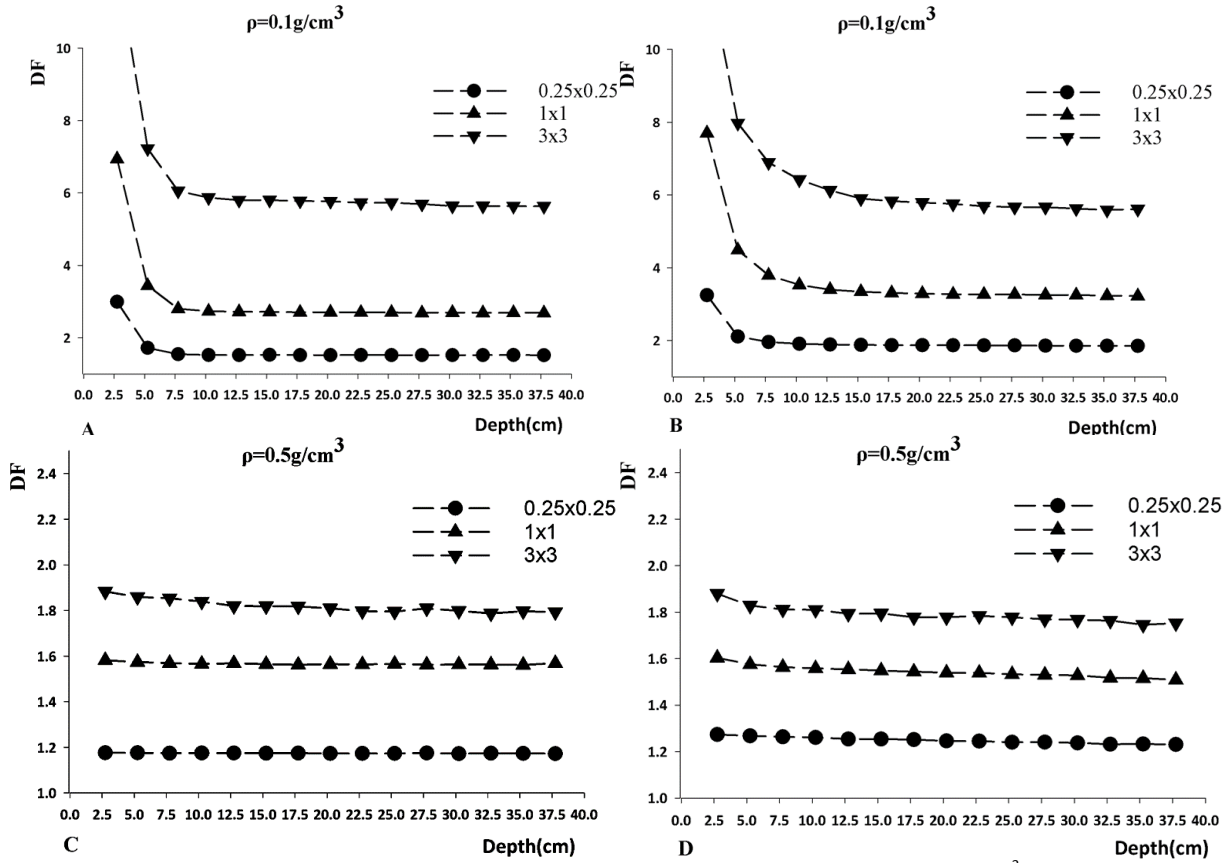


Figure 2. Density factors (DFs) vary with the depth of lung phantoms of density 0.1 **(A, B)** and 0.5 g/cm^3 **(C, D)** for 0.25×0.25 cm^2, 1×1cm^2 and 2×2cm^2 field sizes using 2 MeV **(A, C)** and 6 MV **(B, D)** photon beams.

Table 1. The discrepancy of percentage depth-dose calculated using the new algorithm and DOSXYZnrc.

Depth (cm)	0.25×0.25 cm^2		1×1 cm^2		2×2 cm^2	
	2MeV	6MV	2MeV	6MV	2MeV	6MV
10	0.03	0.19	0.03	0.03	0.19	0.08
12	0.03	0.08	0.12	0.38	0.03	0.01
14	0.05	0.13	0.08	0.42	0.22	0.11
16	3.31	1.66	4.05	1.95	3.5	4.81
18	2.34	0.63	0.37	1.81	0.11	0.12
20	2.05	0.45	0.08	2.06	0.52	1.28
22	1.75	0.32	0.4	2.55	1.03	1.37
24	1.48	0.21	0.64	2.74	1.2	1.9
26	0.03	0.41	1.45	1.46	1.92	2.1
28	0.01	0.18	0.18	0.23	0.92	0.7
30	0.05	0.12	0.12	0.1	0.37	0.41

[Downloaded from mail.ijrr.com on 2026-11-12]

[DOI: 10.52547/ijrr.19.2.3]

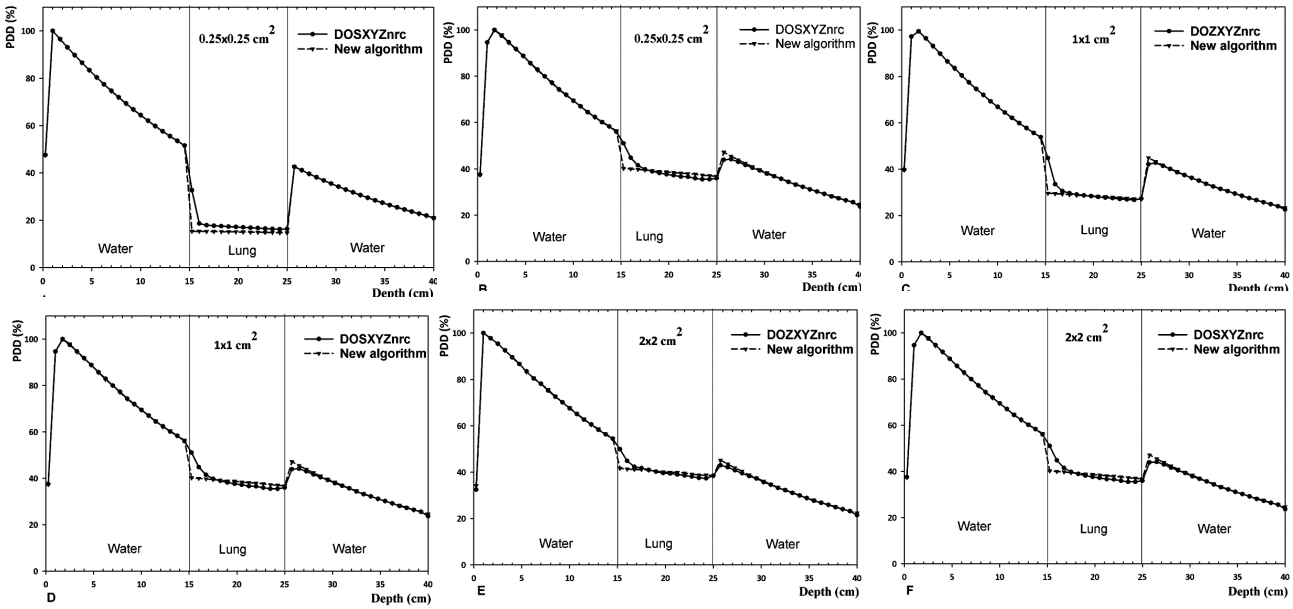


Figure 3. A comparison of percentage depth-dose calculated using the new algorithm (the green dashed line) and Monte Carlo simulations (the red solid line) in heterogeneous lung phantoms with different field sizes using 2 MeV **(A, C, E)** and 6 MV **(B, D, F)** photon beams at a density of 0.26 g/cm^3. **(A, B)** 0.25×0.25 cm^2 **(C, D)** 1×1 cm^2 **(E, F)** 2×2 cm^2].

The PDD curves that vary with energy have also been compared. Figure 3A, C, and E represent the PDD curves in a 2 MeV photon beam, and figure 3B, D, and F represent depth-dose curves in a 6MV photon beam. When the field size was 1×1cm^2 and 2×2 cm^2, the discrepancy in table 1 shows that results with 2 MeV of energy are more accurate than with 6 MV of energy, but when the field size was 0.25×0.25cm^2, the PDDs calculated by the new algorithm in a 6MV of energy were more accurate when calculated with 2 MeV of energy.

In addition, the different locations and thicknesses of the lung in inhomogeneous phantoms are also compared. Figure 4 and table 2 show the different location of the lung part in heterogeneous phantoms. Figure 5 and table 3 show the various thicknesses of the lung tissue in heterogeneous phantoms.

Table 2. The discrepancy of percentage depth-dose for different depths of lung tissue in phantom calculated using the new algorithm and DOSXYZnrc.

Depth (cm)	Depth at 5cm (%)		Depth (cm)	Depth at 25cm (%)	
	2MeV	6MV		2MeV	6MV
3	0.08	0.16	23	0.01	0.04
4	0.08	0.16	24	0.02	0.15
5	0.6	0.65	25	0.2	0.2
7	2.72	2.35	27	1.01	0.25
9	2.42	1.94	29	0.9	0.09
11	2.21	1.61	31	0.82	0.18
13	1.99	1.35	33	0.77	0.07
15	2.31	1.63	35	0.87	0.02
16	0.11	0.6	36	0.04	0.2
17	0.08	0.56	37	0.02	0.06
18	0.05	0.1	38	0.01	0.03

Table 3. The discrepancy of percentage depth-dose for different thicknesses of lung tissue in phantom calculated using the new algorithm and DOSXYZnrc.

Depth (cm)	Thickness=5cm		Depth (cm)	Thickness=15cm	
	2MeV	6MV		2MeV	6MV
13	0.04	0.01	13	0.04	0.03
14	0.01	0.16	14	0.01	0.15
15	0.44	0.37	15	0.44	0.4
16	2.28	1.68	18	1.56	0.66
17	1.67	0.84	21	1.35	0.36
18	1.56	0.62	24	1.15	0.21
19	1.49	0.54	27	0.96	0.01
20	1.75	0.8	30	1.07	0.09
21	0.15	0.39	31	0.14	0.3
22	0.04	0.16	32	0.06	0.04
23	0.04	0.16	33	0.04	0.15

[Downloaded from mail.ijrr.com on 2026-11-12]

[DOI: 10.52547/ijrr.19.2.3]

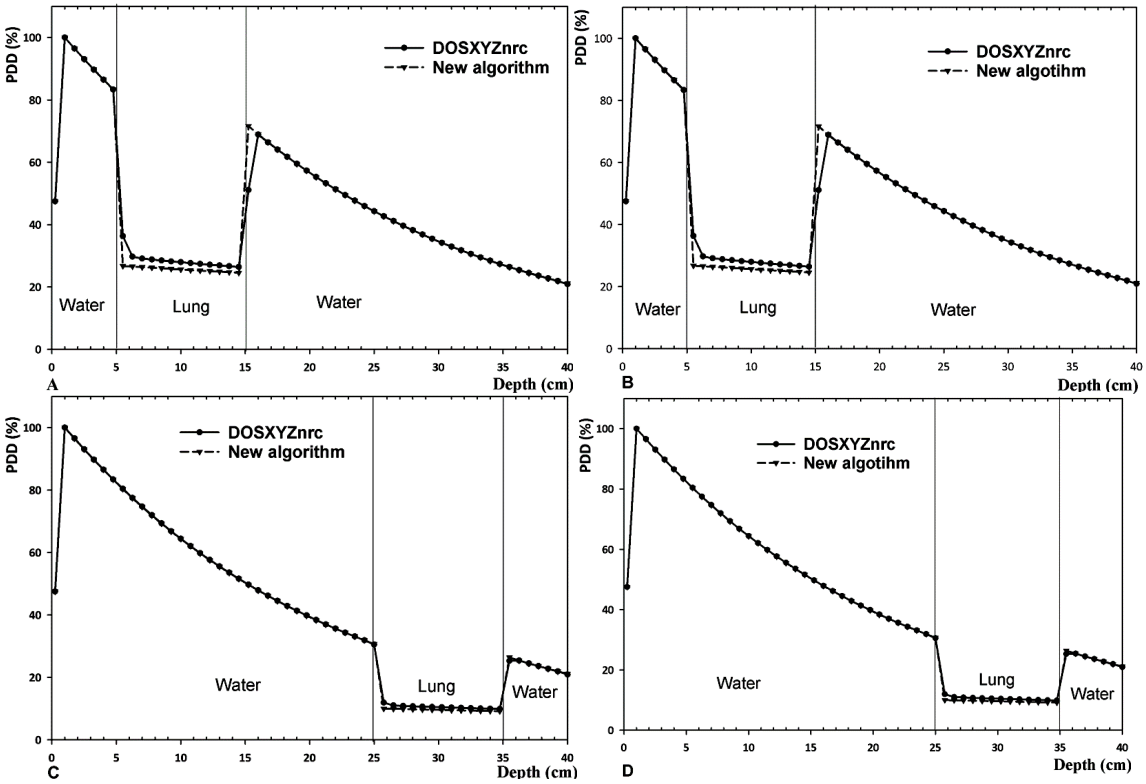


Figure 4. A comparison of percentage depth-dose calculated using the new algorithm (the dashed line) and Monte Carlo simulations (the solid line) in heterogeneous lung phantoms of different depths (5 cm) **(A, B)** and 25cm **(C, D)**) using 2 MeV **(A, C)** and 6 MV **(B, D)** photon beams with a density of 0.26 g/cm^3 for a 0.25×0.25 cm^2 field size.

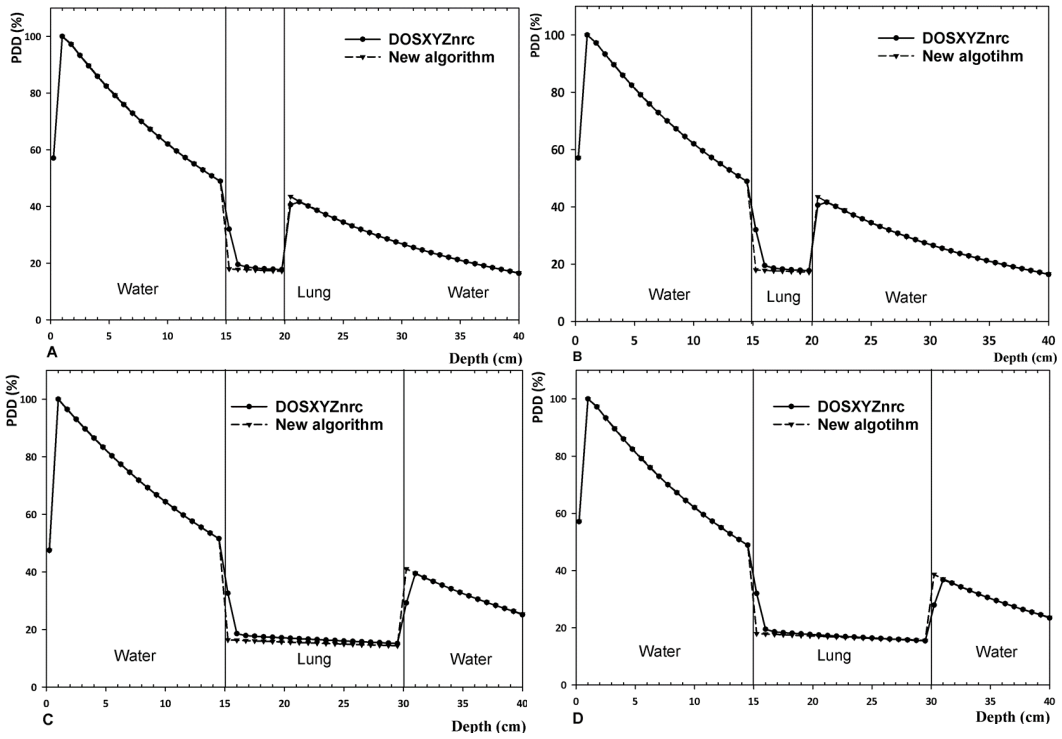


Figure 5. A comparison of percentage depth-dose calculated using the new algorithm (the green dashed line) and Monte Carlo simulations (the red solid line) in heterogeneous lung phantoms of different thicknesses (5cm) **(A, B)** or 15cm **(C, D)**), using 2 MeV **(A, C)** and 6 MV **(B, D)** photon beams with a density of 0.26 g/cm^3 for a 0.25×0.25cm^2 field size.

[Downloaded from mail.ijrr.com on 2026-11-12]

[DOI: 10.52547/ijrr.19.2.3]

All deviations in table 2 are less than 3%; the largest discrepancy is 2.35% at depth of 7cm. When comparing figure 3A, figure 4A and figure 4C, with the depth increase, the discrepancies decrease, and figure 4C shows the minimum deviation and each deviation was less than 1%. With the depth of lung tissue in phantom decrease, the deviations increase.

All deviations in table 3 are also less than 3%; the largest discrepancy is 2.28% at depth of 16cm, and the thickness of the lung tissue in phantom is 5cm. When comparing figure 3A, figure 5A and figure 5C, with the thickness of lung tissue in phantom increase, the deviations have little changed.

DISCUSSION

According to our study, percentage depth-dose distributions in heterogeneous for small field size were calculated using the new algorithm and MC code. The results showed that the PDD distributions in the valley region and the region after the second build-up region agree well with the MC simulations. When the field size decreases, the PDDs calculated by the new algorithm show higher dose deviations; however, these deviations are less than 3%. In the build-down and the second build-up region, the dose deviations show a major discrepancy with MC simulations.

Due to the lack of lateral electronic equilibrium and inhomogeneity, causing a huge impact on dose calculation and measurement. [3,5,19] Lots of researches showed a large dose deviation by using common correction algorithms. In 2015, A. Mesbahi *et al*. [4] compared the full scatter algorithm (FSC) with the MC method. Percentage depth dose curves were calculated in heterogeneous water phantoms with layers of lung (0.25 g/cm^3) equivalent materials for radiation fields between 1×1 cm^2 and 2×2 cm^2. Dose deviations can reach 67% and 33% when using 1 ×1 cm^2 field and 2×2 cm^2 field respectively. For Batho algorithm, du Plessis *et al*. [8] showed absorbed dose deviations of 10–20% in lung tissue of varying density for a 2×2 cm^2 field. Because this algorithm did not consider the transportation of secondary charged particles. In a recent study by Reis C Q M *et al*. [18] MC simulations with PENELOPE package were performed for comparison of doses calculated by pencil beam convolution (PBC) and analytical anisotropy algorithm (AAA). Percentage depth dose curves were calculated in heterogeneous water phantoms with layers of lung (0.3 g/cm^3) equivalent materials for radiation fields between 1×1 cm^2 and 2×2 cm^2. The results calculated by these algorithms showed large dose deviations. For PBC, differences can reach 21.9% on average with a maximum of 24.3% when using a 1 ×1 cm^2 field. At the same conditions, AAA presented an average deviation of 5.8% and maximum of approximately 11.5%. The accuracy of the collapsed cone convolution (CCC) algorithm was relatively high. When the field size was larger than 3×3 cm^2, the dose deviations were less than 3%. But with the field sizes decrease, the dose deviations increase [9]. The American Association of Physicists in Medicine (AAPM) report NO.85 showed that the accuracy of computed dose distributions should be less than 3% [20]. The depth-dose distributions calculated by the above algorithms couldn't be used for clinical treatment when using small fields. But, most dose deviations calculated by the new algorithm were less than 2% when using 1 ×1 cm^2 field and 2×2 cm^2 field.

In conclusion, comparing with these algorithms, the new algorithm mentioned in this study showed a great accuracy. The effects of charged particles' disequilibrium and inhomogeneity were considered in the new algorithm. So, when using small fields, the depth -dose distributions calculated by the new algorithm were more in line with clinical requirements.

ACKNOWLEDGMENTS

This work was supported by the National Key Research and Development Programme of China (grant number 2016YFC0105103). No other potential conflicts of interest relevant to this article were reported.

[Downloaded from mail.ijrr.com on 2026-11-12]

[DOI: 10.52547/ijrr.19.2.3]

Conflicts of interest*: *Declared none.

REFERENCES

1. Partanen M, Ojala J, Niemela J, Bjorkqvist M, Keryrilainen J, Kapanen M (2017) Comparison of two Monte Carlo-based codes for small-field dose calculations in external beam radiotherapy. *Acta Oncol, **56(6)**: 891-897*.
2. Townson R, Egglestone H, Zavgorodni S (2018) A fast jaw-tracking model for VMAT and IMRT Monte Carlo simulations. *J Appl Clin Med Phys, **19(4)**: 26-34*.
3. Saw C B and Li S (2018) 3D treatment planning systems. *Med Dosim, **43(2)**: 103-105*.
4. A Mesbahi and H Dadgar (2015) Dose calculations accuracy of TiGRT treatment planning system for small IMRT beamlets in heterogeneous lung phantom. *Int J Radiat Res, **13(4)**: 345-354*.
5. Xue J, McKay JD, Grimm J, Cheng CW, Berg R, Grimm SQ, *et al.* (2017) Small field dose measurements using plastic scintillation detector in heterogeneous media. *Med Phys, **44**: 3815-3820*.
6. T Knöös, E Wieslander, L Cozzi, C Brink, A Fogliata, D Albers, *et al.* (2006) Comparison of dose calculation algorithms for treatment planning in external photon beam therapy for clinical situations. *Phys Med Biol, **51(22)**: 5785 -5807*.
7. Fogliata A and Cozzi L (2017) Dose calculation algorithm accuracy for small fields in non-homogeneous media: The lung SBRT case. *Phys Medica, **44**: 157-162*.
8. Arnfield MR, Siantar CH, Siebers J, Garmon P, Cox L, Mohan R (2000) The impact of electron transport on the accuracy of computed dose. *Med Phys, **27(6)**: 1266*.
9. Jones AO and Das IJ (2005) Comparison of inhomogeneity correction algorithms in small photon fields. *Med Phys, **32 (3)**: 766*.
10. Fotina I, Kragl G, Kroupa B (2011) Clinical Comparison of Dose Calculation Using the Enhanced Collapsed Cone Algorithm vs. a New Monte Carlo Algorithm. *Strahlenther Onkol, **187(7)**: 433-441*.
11. Vassiliev O N, Wareing T A, Mcghee J, Failla G, Salehpour M R, Mourtada F (2010) Validation of a new grid-based Boltzmann equation solver for dose calculation in radiotherapy with photon beams. *Phys Med Biol, **55(3)**: 581-598*.
12. Lu W, Olivera GH, Chen ML (2005) Accurate convolution/superposition for multi-resolution dose calculation using cumulative tabulated kernels. *Phys Med Biol, **50(4)**: 655-680*.
13. Luo ZM, Gou CJ, Wolfram L (2003) The penetration, diffusion and energy deposition of high—energy photon. *Chin Phys B, **12(7)**: 803-808*.
14. Ford JR, Maslowski AJ, Redd RA (2005) Radiation Responses of Perfused Tracheal Tissue. *Radiat Res, **164(4 Pt 2)**: 487 -492*.
15. Walters BRB, Kawrakow I, Rogers DWO (2016) DOSXYZnrc Users Manual. *NRCC Report PIRS, 794 (rev B)*.
16. Kawrakow I, Mainegra HE, Rogers DWO (2020) The EGSnrc Code System: Monter Carlo Simulation of Electron and Photon Transport, NRCC Report PIRS-701.
17. Jabbari N, Nedaie H, Zeinali A (2011) Evaluation of the electron energy fluence and angular distributions from a clinical accelerator. A BEAMnrc Monte Carlo study. *Int J Radiat Res, **9(1)**:29-36*.
18. Reis CQM, Nucolucci P, Fortes SS, Silva LP (2019) Effects of heterogeneities in dose distributions under nonreference conditions: Monte Carlo simulation vs dose calculation algorithms. *Med Dosim, **44(1)**: 74-82*.
19. Das I J, Ding G X, Ahnesj A (2008) Small fields: Nonequilibrium radiation dosimetry. *Med Phys, **35(1)**: 206-215*.
20. Sharpe MM and Van Dyk J (2004) Tissue inhomogeneity corrections for megavoltage photon beams, AAPM report No 85, Task Group No 65 of the Radiation Therapy Committee of the American Association of Physicists in Medicine.

[Downloaded from mail.ijrr.com on 2026-11-12]

[DOI: 10.52547/ijrr.19.2.3]

[DOI: 10.52547/ijrr.19.2.3] [Downloaded from mail.ijrr.com on 2026-11-12]